ISOCAM FIELD DISTORTION REPORT

K. Okumura[1]

November 7, 2000

1 : IAS, Université Paris XI, Bât.121, 91405 Orsay Cedex, France

version : 1.0

1 Introduction

ISOCAM images present a field distortion whose amplitude depends on the lens which determines the pixel-field-of-view (pfov) of the image. Larger the pfov severer the distortion. It is important to correct for this instrumental effect especially when making a coadded map from a raster observation. The correction is made by means of a polynomial pair which relates the distorted two-dimensions space to a distortion-free two-dimensions space. During first years of data reduction, only a few polynomial coefficients were available. They were directly derived from observations in a few configurations (Aussel 1998 [1] and 1999 [2]).

Table. 1 lists the observations used for the derivation of the field distortion coefficients. The third column indicates whether a dark column is seen at the right edge of the image in the current CIA (*CAM Interactive Analysis*) convention. Namely, horizontal axis is in the projected (Y) axis and vertical axis is in the projected ($-Z$) axis. This dark column appears when the extended background emission is strong enough. This is one of the field mirror edges seen often on the right hand depending on the lens wheel position which varies in the limit of tolerance. When a right column is not seen, Table. 1 indicates "right" and when it is seen, it indicates "left". The fourth column of Table. 1 gives the type of data. The Gamma ray burst data have various point sources in one CAM filed, and in addition a larger field is observed in a raster. On the contrary, Ghosts data are rasters around only one bright point source. Both of them can give spatial distribution of point sources over the detector with their "ideal" positions.

Table 1: Observations used for the field distortion correction polynomials derivation

PFOV	filter	lens	data
6 arcsec	LW10 10.67μm	left	Gamma ray burst
6 arcsec	LW10 10.67μm	right	Gamma ray burst
6 arcsec	LW3 13.99μm	?	Ghosts
6 arcsec	CVF1 7μm	?	Ghosts
6 arcsec	CVF2 12μm	?	Ghosts
3 arcsec	LW10 10.67μm	right	Gamma ray burst
3 arcsec	LW2 6.36μm	?	Ghosts
3 arcsec	LW3 13.99μm	?	Ghosts

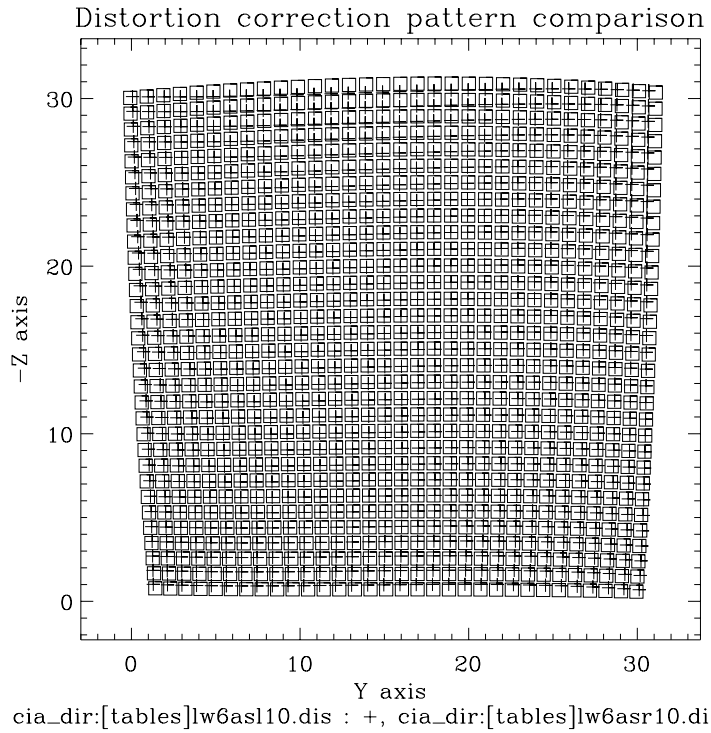

Figure 1: Comparison of distortion correction pattern (correction applied to a regular grid) between 2 different lens wheel positions according to H.Aussel

Table 2: Different effects of the optical elements in the field distortion

Elements	**Distortion effect**
field mirror tilt	trapezoidal deformation
lens aberration	pin cushion distortion
filter width	magnification

A third order polynomial pair is fitted between the observed and "ideal" positions. The lens position is thought to influence substantially the distortion (see Fig. 1). At this stage, CIA uses the nearest configuration for the distortion correction. However the distortion seems to be different for different filters, suggesting a wavelength dependency. Unfortunately, there are not enough calibration observations to cover every filters. Hence, it is important to develop an optical model to derive a complete set of polynomials.

2 How does the field distortion occur?

The field distortion in ISOCAM is due to all optical elements the beam encounters: field mirror, filter and lens. Each of these elements acts in a different way and to a different extent. Table. 2 lists different effect for each optical element.

The trapezoidal deformation observed in the distortion pattern is due to the inclination of the Fabry field mirror. This effect is reproduced in a simple first order optical computation (Fig. 2).

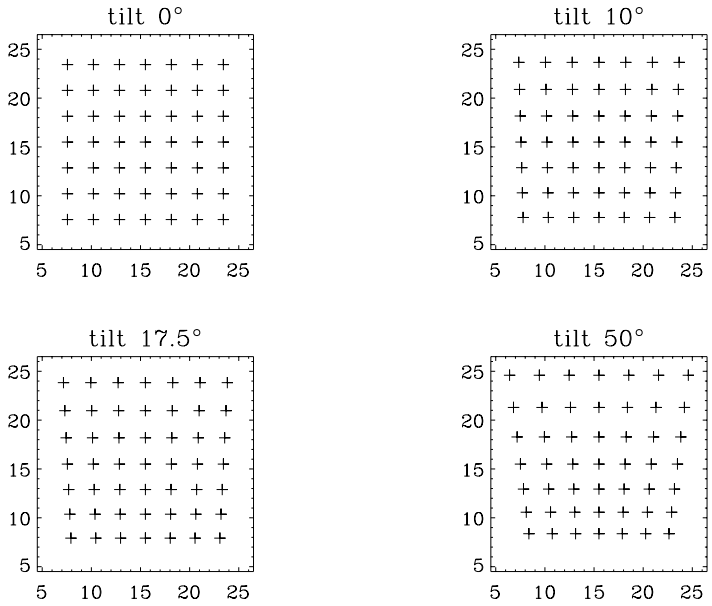

Figure 2: In the first order optics (Descartes's approximation) a tilt of the field mirror gives a trapeze

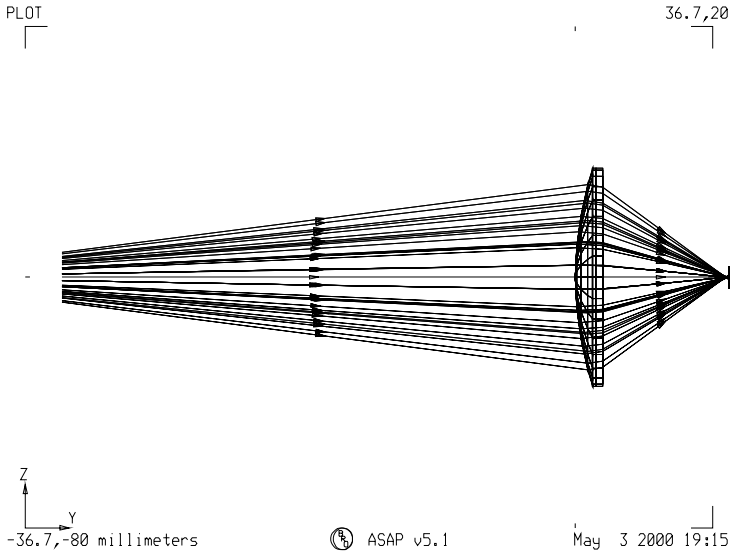

Figure 3: If one consider a beam 4 times larger than the real one so that a large fraction of 12 arcsec pfov lens surface is covered, then...

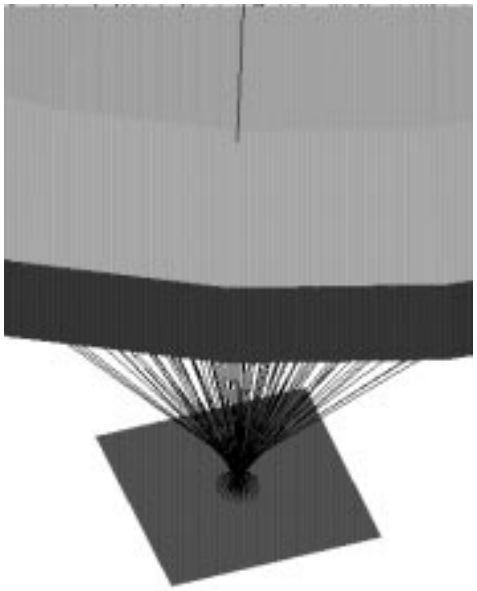

Figure 4: ..., then the focusing is as bad as this!

The pincushion distortion occurs when the beam passes through the lens. This effect arises from the aspherical aberration of the lens. Therefore, the first order computation is not sufficient. One can reproduce this effect in a ray tracing computation (Fig. 3 and Fig. 4). The width of the filter plates contribute also in a magnification change. As the beam is converging when passing through the filter, the parallel planes of the filter plates (inclined or not) have an influence on the field pattern on the detector.

3 Extension of distortion measurements and comparison with ASAP simulations

In order to elaborate an optical model which can reproduce the distortion pattern, some parameters should be adjusted by comparing with observations. For this purpose, more extended distortion measurements have been performed. Table. 3 shows the data used for the new measurements. Except for the 12 arcsec PFOV, all the data are from ghosts measurements performed for the calibration use[1].

The data for 12 arcsec PFOV are five rasters centered on five different positions over the detector array. Micro scanning of 3 arcsec step size in each position is ignored and only the central positions of the micro rasters are used. As mentioned above, 12 arcsec PFOV lens presents a most serious distortion. Therefore, it is important to have a test case with this lens. Fig. 5 shows a significant difference of distortion between LW1 (4.44μm) and LW3 (13.99μm) filters. The 6 arcsec PFOV lens does not show such a big difference, but more data are available in different wavelengths. A preliminary comparison between the ASAP optical model and the observations

[1] For the data identification, see ISOCAM PSF report [3] and Ghosts in ISOCAM images [4]

Table 3: New field distortion measurements

PFOV	filter	positions	observations
1.5	LW2 6.36μm	5×5	Ghosts
1.5	LW3 13.99μm	5×5	Ghosts
1.5	CVF2 9μm	5×5	Ghosts
1.5	CVF2 12μm	5×5	Ghosts
1.5	CVF2 15μm	5×5	Ghosts
3, 6	LW1 4.44μm	9×9	Ghosts
3, 6	LW2 6.36μm	9×9	Ghosts
3, 6	LW3 13.99μm	9×9	Ghosts
3, 6	LW7 9.49μm	9×9	Ghosts
3, 6	LW10 10.67μm	9×9	Ghosts
3	CVF1 5μm	6×4	Ghosts
3	CVF1 7μm	6×4	Ghosts
3	CVF1 9μm	6×4	Ghosts
3	CVF2 9μm	6×4	Ghosts
3	CVF2 12μm	6×4	Ghosts
3	CVF2 15μm	6×4	Ghosts
6	CVF1 5μm	9×5	Ghosts
6	CVF1 7μm	9×5	Ghosts
6	CVF1 9μm	9×5	Ghosts
6	CVF2 9μm	9×5	Ghosts
6	CVF2 12μm	9×5	Ghosts
6	CVF2 15μm	9×5	Ghosts
12	LW1 4.44μm	5 rasters	PSFs
12	LW3 13.99μm	5 rasters	PSFs

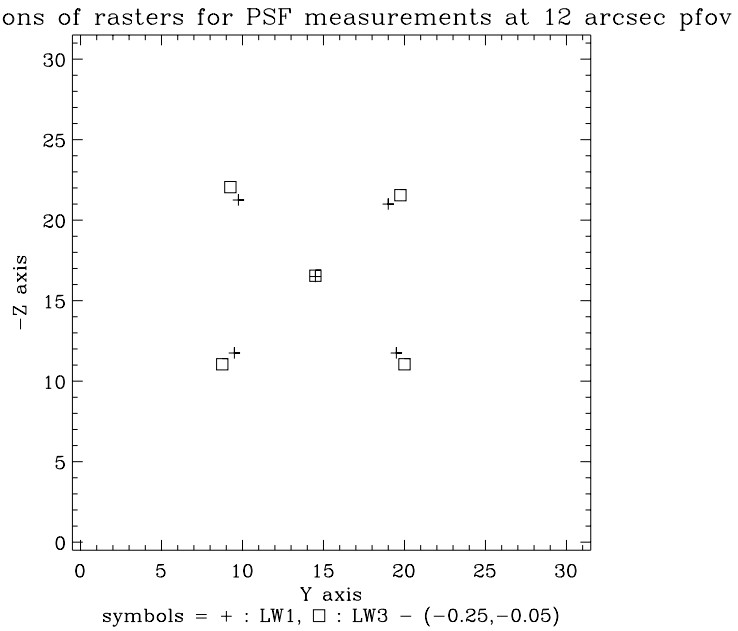

Figure 5: Raster central positions of PSF measurements through 12 arcsec PFOV lens at LW1 and LW3

has demonstrated the need for adjusting some parameters in the model. After putting realistic widths of filters in the model, and after some trials, it seemed natural to try to adjust the refractive index of the germanium in order for the model to give distortions comparable to the observations. Germanium is the material used for all the lenses of the LW channel and a part of filters. Its refractive index is not known within a good accuracy at the operational temperature of ISOCAM. Comparisons between the model and some observations allows to determine this quantity over the CAM's wavelength range. However, one should bear in mind that the refractive index determined in this way is not a real one, since there are other materials such as calcium fluoride or sapphire in some filters whose refractive index is as uncertain as that of germanium. The adjusted values of the refractive index of germanium should be regarded as a simple model parameter which minimize the deviation from the observations.

3.1 Refractive index as a function of the wavelength

The configurations which allow distortion measurements with least error would be those with 12 arcsec PFOV lens because of their large distortion. However, because of the scarcity of observations using this lens, most calibration observations have been done with the other lenses. The PSFs observations through 12 arcsec PFOV lens are used only for the central positions of the rasters. The position of each raster is then affected by the absolute pointing error, whereas the ghosts measurements through the other lenses are done by one raster observation which is affected only by the relative pointing error. The best data set to investigate the wavelength dependency of the field distortion is the 6 arcsec PFOV lens in this situation.

Fig. 6 shows an example of the comparison of point source observed by a raster and the corresponding result given by ASAP optical model. By adjusting the value of refractive index for each wavelength (5, 7, 9, 9, 12 and 15 μm in the data set), one can obtain the best match of the raster size (Fig. 7). Fig. 8 shows the variation of the refractive index as a function of the wavelength. The global shape of this curve is reproduced by an exponential function. If

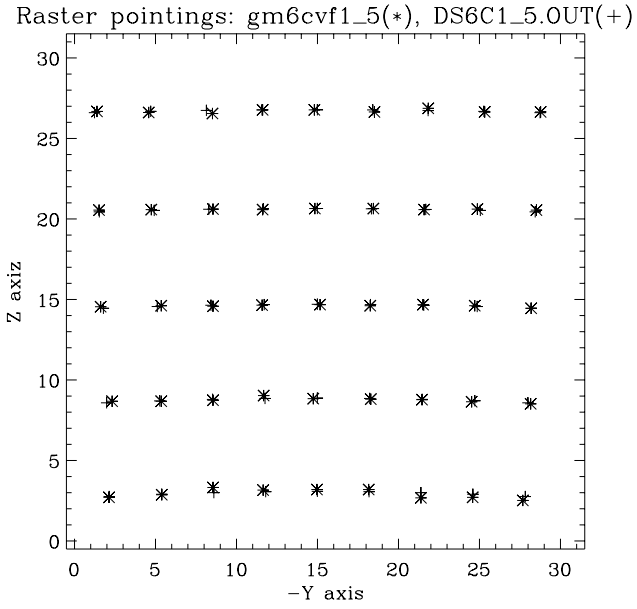

Figure 6: Example of a comparison model-observation of the 9×5 raster points through 6 arcsec pfov lens at 5 μm (CVF1)

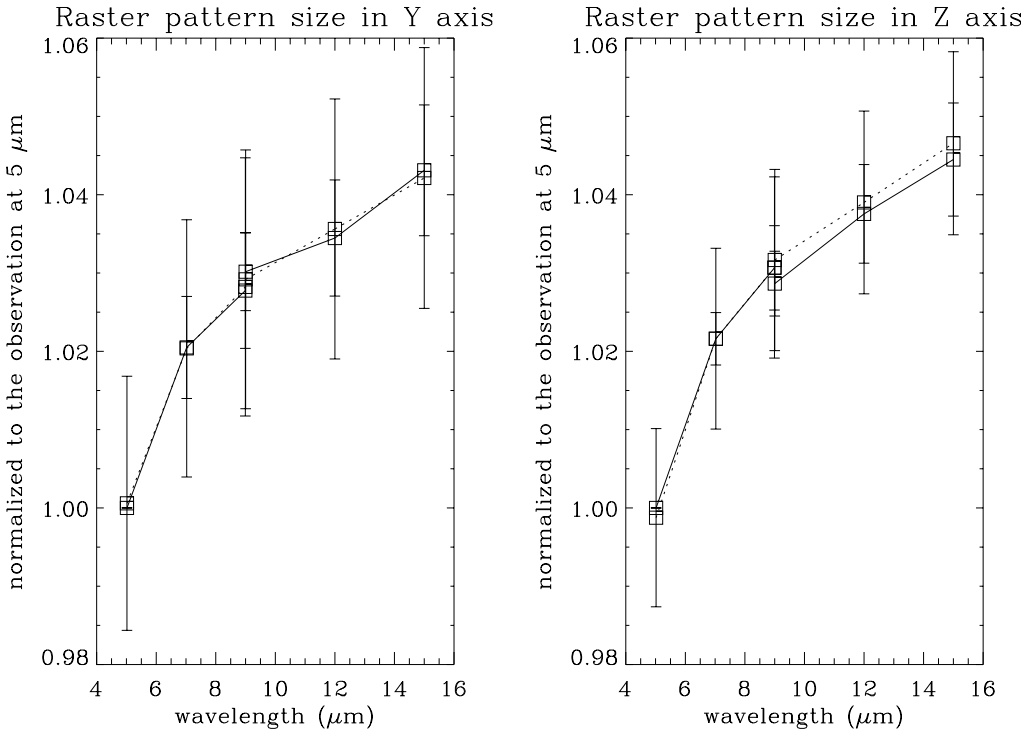

Figure 7: Raster size as a function of the wavelength through the CVFs, measurements and model with reasonable choice of the refractive index

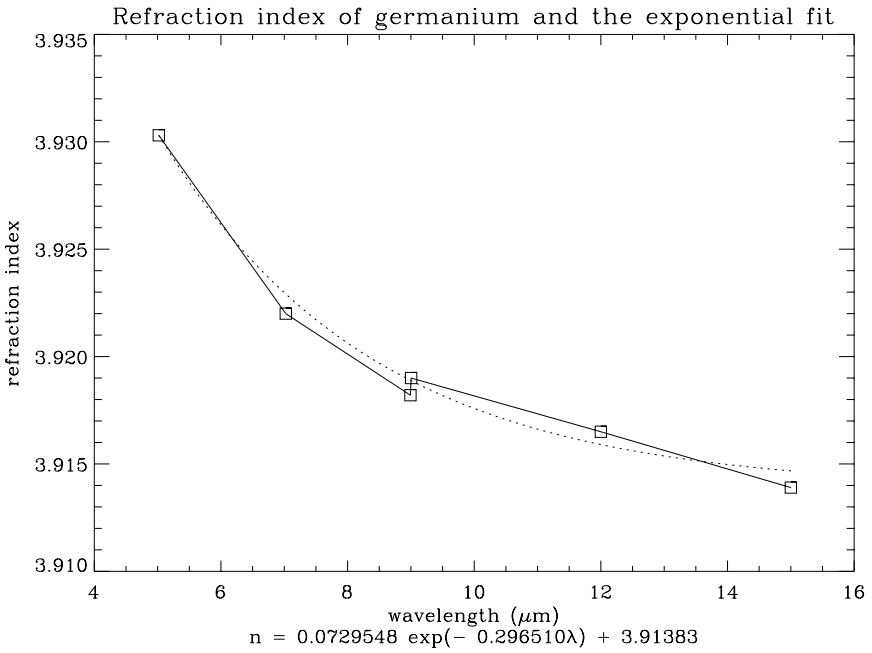

Figure 8: An exponential interpolation on the refractive index as a function of the wavelength

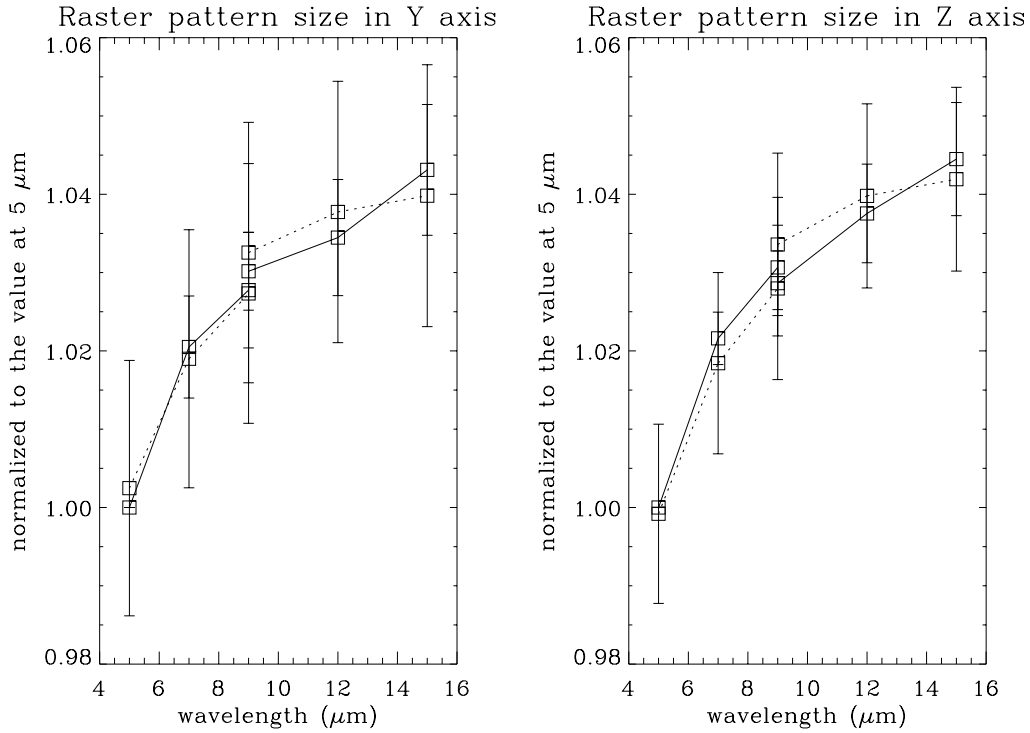

Figure 9: Raster size as a function of the wavelength through the CVFs, measurements and model with an exponential interpolation on the refractive index

Table 4: Observations which show the size of the field mirror on the detector

PFOV	field mirror	filter	TDT No.	observations
6	small	LW9 15.02μm	25804002	Flat
6	small	LW9 15.02μm	25804103	Flat
6	small	LW9 15.02μm	25804204	Flat
6	small	LW9 15.02μm	25804305	Flat
6	small	LW9 15.02μm	25804406	Flat
6	small	LW9 15.02μm	25804507	Flat
6	small	LW9 15.02μm	25804608	Flat
6	small	LW9 15.02μm	25804709	Flat
6	small	LW9 15.02μm	25804810	Flat
6	small	CVF2 15.0μm	25804911	Flat
6	small	CVF2 15.0μm	25805012	Flat
6	small	CVF2 15.0μm	25805214	Flat
6	small	CVF2 15.0μm	25805416	Flat
6	small	CVF2 15.0μm	25805618	Flat
12	large	LW2 7.35μm	41205409	Flat
12	large	LW3 15.18μm	41204803	Flat
12	large	LW9 15.02μm	41205005	Flat
12	large	LW10 12.82μm	41205611	Flat
12	large	CVF2 15.0μm	46104403	Flat
12	large	CVF2 11.37μm	46104403	Flat
12	large	CVF1 7.687μm	46104403	Flat
12	large	LW9 15.02μm	46104403	Flat
12	large	LW8 11.39μm	46104403	Flat
12	large	LW6 7.87μm	46104403	Flat

this exponential function is adopted the optical model gives a reasonable raster size variation relative to the wavelength (Fig. 9).

3.2 Field distortion models versus observations

For the refractive index adjustment, additional data can be helpful. In observations which use 12 arcsec PFOV lens or 6 arcsec PFOV lens with the small field mirror, the field mirror edges can easily be seen (Table. 4). The observed mirror size gives us a partial information about the field distortion. The wavelengths covered by these flat observations does not go shorter than 7.35 μm due to the low brightness level of the zodiacal light in the shorter wavelength range. The distortion variation through 12 arcsec PFOV lens must be quite noticeable in this wavelength range and especially in this outer limits of the field. However, due to the large uncertainty on the measure of the field mirror border, this is not easily seen. These data still provide an important check with independent data which are different from those with point source data of Table. 3. The observed mirror sizes are consistent with those given by the optical simulations in the limit of the error of measurement.

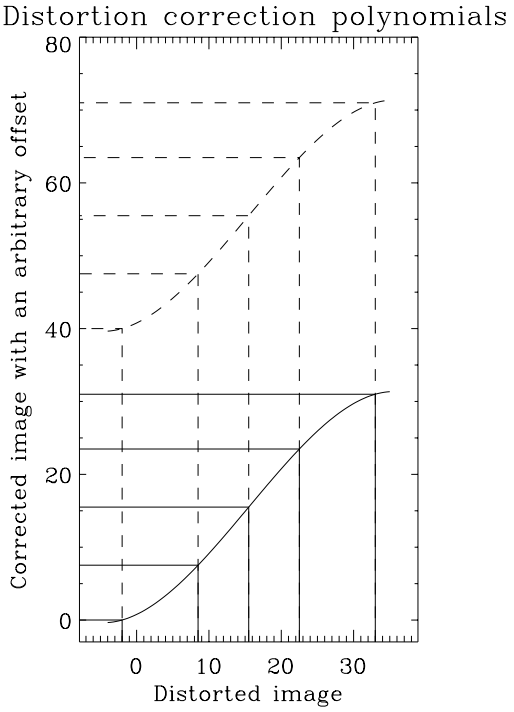

Figure 10: Distortion correction polynomials

4 Offset convention for the field distortion polynomials

As mentioned before, the field distortion is corrected by third order polynomials. However, the polynomial coefficients changes if the origin of the image coordinates change. Therefore, a clear standard convention of the origin is needed in order to avoid any confusion.

Due to the uncertainty on the lens wheel position, the intersection of the optical axis with the detector is not known *a priori* with an accuracy better than $\approx$ 18 arcsec in Y axis direction. However, this position is important for the distortion pattern measured with point sources placed over the detector. For a given position of the lens wheel, this pattern is, in some sens, "centered" at the optical axis on the detector. In principle, this point is where the distortion is less severe. Therefore this point should be taken as the astrometric reference point of the image. Nevertheless, since this point is not well known for each observation, a fixed position has to be taken as the astrometric reference point. In some cases, this reference point is off from the real optical axis up to a few pixel. However this offset is confined in the central part of the detector and it does not introduce more than 1% error.

In the following, (X, Y) represent coordinates values in a known projection grid space. (x, y) stand for coordinates values in the distorted space, which correspond to the real position on the detector. (P_x, P_y) are the distortion correction polynomials which transform (x, y) to (X, Y) and (P_x^{-1}, P_y^{-1}) are the distortion generation polynomials which give (x, y) from (X, Y). The ranges of (X, Y) are, in general, defined by the detector dimensions in the pixel numbering convention of an used image processing package. In the case of CIA, this convention follows that of IDL language, *e.i.* $(0, 0)$ to $(31, 31)$. The astrometric reference point is defined at $(15.5, 15.5)$ in CIA[2]. Once one convention of pixel numbering is adopted, the coordinate origin is fixed. On

[2]However the fields CRPIX1 and CRPIX2 of the CIA data are set to 16.5 according to the FITS convention

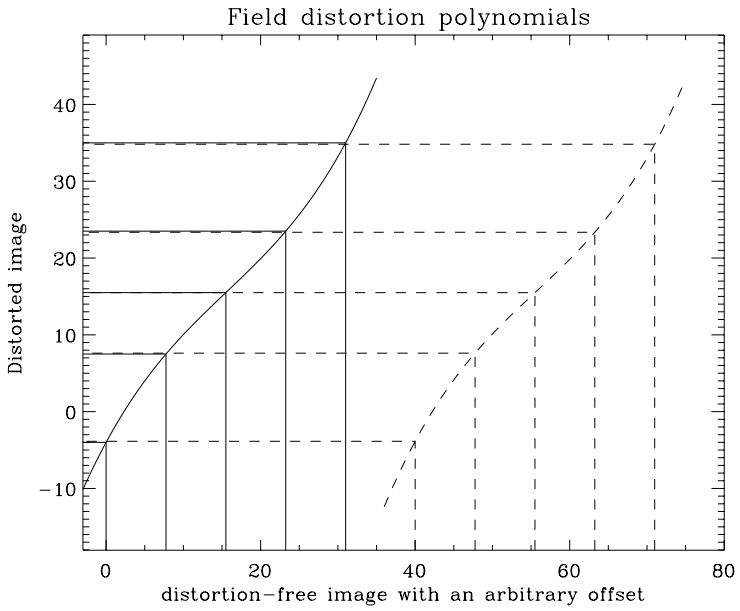

Figure 11: Distortion generation polynomials

the contrary, the corresponding position in (X, Y) space has no privileged values except that this should be decided by taking into account the grid range of the corrected image and its astrometric reference point.

Let us suppose that one clear convention is adopted and this defines a standard polynomial pair. To start with, a polynomial pair can be defined with an arbitrary origin of (X, Y) coordinates space. From this polynomial pair (p_x, p_y), a standard polynomial pair (P_x, P_y) can be derived by applying an offset (a, b) to (X, Y) (Fig. 10 illustrates this situation in one dimension).

$$\begin{cases} X - a &= p_x(x, y) \\ Y - b &= p_y(x, y) \end{cases}$$

The standard polynomial pair (P_x, P_y) is given by:

$$\begin{cases} X &= P_x(x, y) &= p_x(x, y) + a \\ Y &= P_y(x, y) &= p_y(x, y) + b \end{cases}$$

where the offset (a, b) is given by:

$$\begin{cases} a &= X_0 - p_x(x_0, y_0) \\ b &= Y_0 - p_y(x_0, y_0) \end{cases} \tag{1}$$

where (x_0, y_0) is the astrometric reference point in the observed distorted image, and (X_0, Y_0) is that of the corrected image which may be different from (x_0, y_0) according to the detector size after correction. Once (a, b) are determined, the transformation from (p_x, p_y) to (P_x, P_y) is straightforward, because it implies only a change in the constant terms of the polynomial pair.

which begins the pixel numbering from 1 instead of 0.

Now, the standard polynomial pair of the inverse transformation is obtained in a different way. An offset should be applied always to (X, Y) (Fig. 11 illustrates this situation in one dimension). This leads to consider a transformation:

$$\begin{cases} x = P_x^{-1}(X, Y) = p_x^{-1}(X - a, Y - b) \\ y = P_y^{-1}(X, Y) = p_y^{-1}(X - a, Y - b) \end{cases} \quad (2)$$

In the limit of polynomial fitting error, (a, b) are the same as those determined above, but the computation of the coefficients of (P_x^{-1}, P_y^{-1}) is not as simple as those of (P_x, P_y). This transformation changes all the polynomial coefficients except for those of the highest order.

For the sake of the simplicity, only one convention is adopted for all configurations by taking $(x_0, y_0) = (16.5, 16.5)$ and $(X_0, Y_0) = (16.5, 16.5)$ in FITS convention and by adopting the gnomonic projection in the distortion corrected space. The point $(x_0, y_0) = (16.5, 16.5)$ is the defined reference point in CIA in the parameter CRPIXs, which corresponds to the detector center (15.5, 15.5) in the IDL index.

However, users might want to use other values of (x_0, y_0) and (X_0, Y_0). For instance, one might want to put a distortion corrected image centered at (α, β) different from the standard position $(16.5, 16.5)$. The offset can be computed by Eq. 1, and then the constant terms of the polynomial pair should be modified by adding (a, b). On the other hand, from a distortion-free map of well known projection, one might want to extract an area at whatever position (α, β) corresponding to a ISOCAM filed of view and try to simulate a distorted image seen by ISOCAM. After a preliminary operation to put this area in the gnomonic projection, one should use the coefficients of (P_x^{-1}, P_y^{-1}) computed for the position $(X_0, Y_0) = (\alpha, \beta)$. However, this transformation changes all the coefficients except for those of the highest order. The coefficients can be computed by developing the expression:

$$p^{-1}(x, y) = \sum_{k=0}^{n} \sum_{i=0}^{k} C_{i,k-i}(X - X_0)^i (Y - Y_0)^{k-i}$$

Another option is to perform a preliminary coordinate offset and use the standard polynomial coefficients. First, the coordinates offset (a, b) is determined by the equation 1. Then one can use the standard coefficients of (P_x^{-1}, P_y^{-1}) by a variable change $(X - a, Y - b)$ as in Eq. 2, instead of computing the new coefficients.

5 Application of correction to 12 arcsec PFOV data

Once the field distortion polynomials are determined, the field distortion correction can be applied. Fig. 12 shows an example of the comparison between the field distortion correction pattern derived from the data and that derived from the optical model at 6 arcsec PFOV.

In the data through 12 arcsec PFOV lens, there are only 5 positions available. The number of polynomial coefficients of the order d is given by the following formula.

$$N_{\text{coeff}} = \frac{(d+1)(d+2)}{2}$$

For third order polynomials, more than 10 positions are needed. Therefore, there are not enough points to compute third order polynomials with 12 arcsec PFOV lens data set. Only first order polynomials can be fitted to 5 positions. However, once the refractive index is determined with data at 6 arcsec PFOV, it is possible to use the optical model for the 12 arcsec PFOV. One

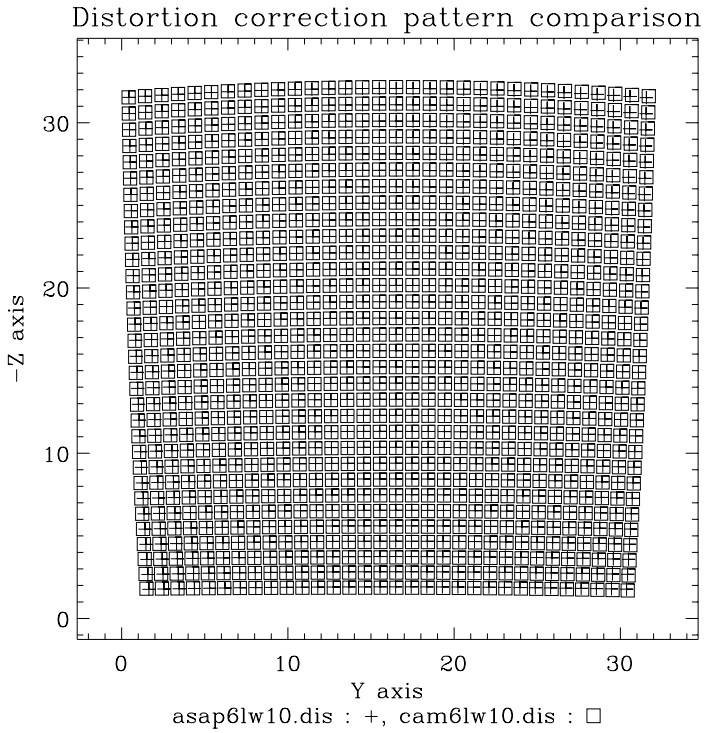

Figure 12: Comparison between observation and model for LW10 at 10.67μm through 6 arcsec PFOV

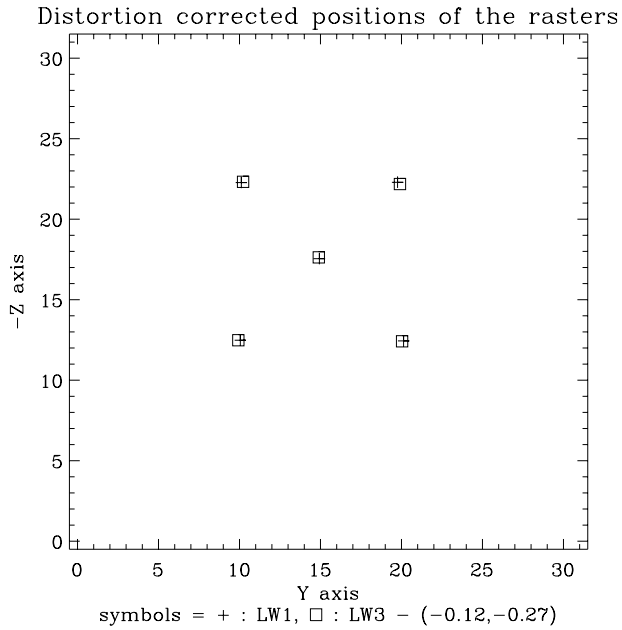

Figure 13: Distortion corrected raster central positions of PSF measurements through 12 arcsec PFOV lens at LW1 and LW3

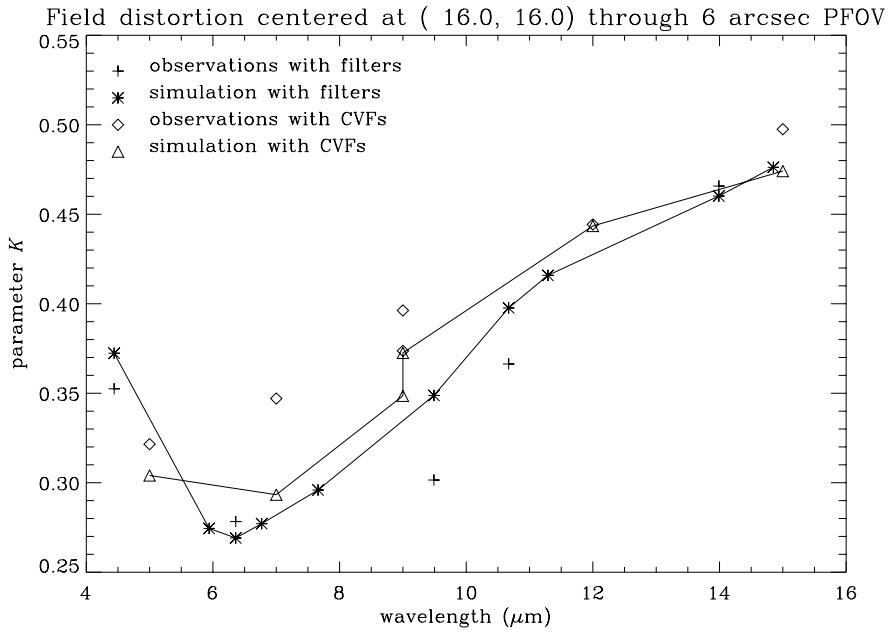

Figure 14: Distortion intensity K computed for a optical axis

can take as many positions as one needs in the model. It allows to reach more accuracy, as long as the parameters in the model are well determined. Fig. 13 shows the distortion corrected positions of the Fig. 5 using the third order polynomials derived from the optical model whose refractive indices are tuned on data through 6 arcsec PFOV lens.

6 Parameters for the analysis of the field distortion

In order to compare the distortion polynomials at different wavelengths, it is convenient to compute a parameter which characterizes the distortion. One of such parameters is the standard deviation K of the distorted image from the distortion-free image computed over the detector surface.

$$K = \sqrt{\frac{\int_{x_{\rm inf}}^{x_{\rm sup}} \int_{y_{\rm inf}}^{y_{\rm sup}} [(P_x(x,y)-x)^2 + (P_y(x,y)-y)^2]\, dx\, dy}{(x_{\rm sup}-x_{\rm inf})(y_{\rm sup}-y_{\rm inf})}}$$

where P_x and P_y are a polynomial pair with the standard origin convention.

$$P_x(x,y) = \sum_{n=1}^{d} \sum_{i=0}^{n} a_{i,n-i} x^i y^{n-i}$$

$$P_y(x,y) = \sum_{n=1}^{d} \sum_{i=0}^{n} b_{i,n-i} x^i y^{n-i}$$

and for 1.5, 3 and 6 arcsec PFOV lenses

$$\begin{cases} x_{\rm inf} = y_{\rm inf} = 0 \\ x_{\rm sup} = y_{\rm sup} = 31 \end{cases}$$

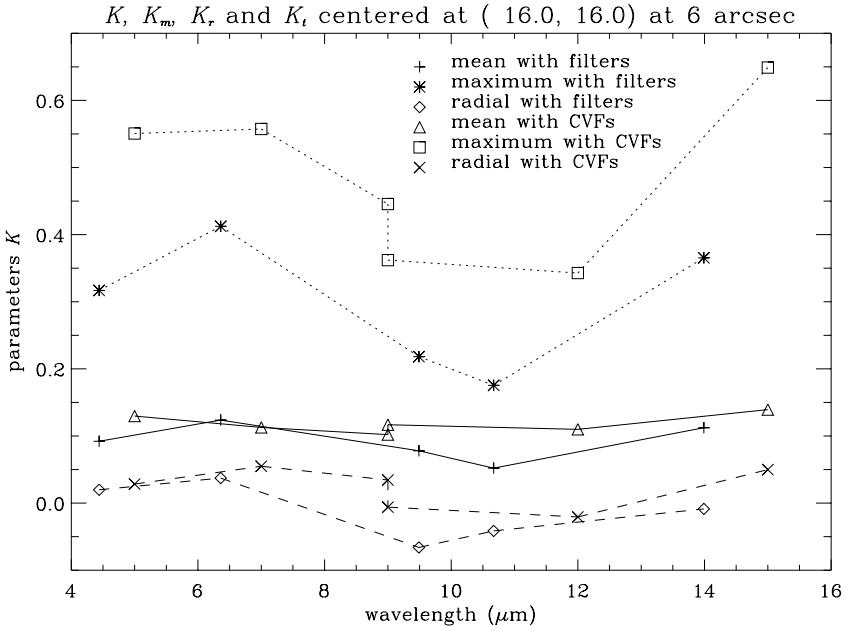

Figure 15: Different parameters Ks to compare the model and data

whereas for 12 arcsec PFOV lens

$$\begin{cases} x_{\inf} = y_{\inf} = 8 \\ x_{\sup} = y_{\sup} = 23 \end{cases}$$

The parameter K has an advantage of being easily computed in the analytical way from the polynomial coefficients. However, it is important to know that K is strongly dependent on the adopted origins. If the distance between (x_0, y_0) and (X_0, Y_0) is larger than a few pixels, the parameter K measures mainly the global offset between the origins. The polynomials with the standard convention give a reasonable parameter K of the field distortion. Fig. 14 shows the variation of the distortion measured by the parameter K as a function of the wavelength.

The same quantity is computed to compare two different distortions represented by $(P_x(x,y), P_y(x,y))$ and $(P'_x(x,y), P'_y(x,y))$.

$$K = \sqrt{\frac{\int_{x_{\inf}}^{x_{\sup}} \int_{y_{\inf}}^{y_{\sup}} \left[(P'_x(x,y) - P_x(x,y))^2 + (P'_y(x,y) - P_y(x,y))^2 \right] dx\,dy}{(x_{\sup} - x_{\inf})(y_{\sup} - y_{\inf})}}$$

The parameter K is an average value over the detector. It is useful to have some idea about the maximum distortion on the detector. This can be reasonably defined by taking the maximum distance at 4 corners of the detector. For a distortion, this parameter K_m is computed by:

$$K_m = \mathrm{Max}(\sqrt{(P_x(x,y) - x)^2 + (P_y(x,y) - y)^2})$$

and for two distortions:

$$K_m = \mathrm{Max}(\sqrt{(P'_x(x,y) - P_x(x,y))^2 + (P'_y(x,y) - P_y(x,y))^2})$$

Now, K and K_m give an idea of the distortion or of the difference between two patterns, but they do not tell in which way they are different, for instance which of them has a larger

magnification, or if one of them is rotated with respect to the other. In order to represent more information about the distortion, one can compute the mean value of the difference vectors projected on the radial K_r and tangential K_t direction relative to a given center.

$$\begin{cases} K_r &= \frac{\int_{x_{\rm inf}}^{x_{\rm sup}} \int_{y_{\rm inf}}^{y_{\rm sup}} d\vec{P}\cdot\vec{U}_r dxdy}{(x_{\rm sup}-x_{\rm inf})(y_{\rm sup}-y_{\rm inf})} \\ K_t &= \frac{\int_{x_{\rm inf}}^{x_{\rm sup}} \int_{y_{\rm inf}}^{y_{\rm sup}} d\vec{P}\cdot\vec{U}_t dxdy}{(x_{\rm sup}-x_{\rm inf})(y_{\rm sup}-y_{\rm inf})} \end{cases}$$

where $d\vec{P} = (P_x - x, P_y - y)$ for a distortion and $d\vec{P} = (P'_x - P_x, P'_y - P_y)$ for two distortions. $(\vec{U}_r, \vec{U}_t)$ are the unit vectors in the radial and tangential direction with respect to a given origin $\vec{o} = (x_0, y_0)$.

$$\begin{cases} \vec{U}_r &= (U_{rx}, U_{ry}) = \frac{\vec{P}-\vec{o}}{|\vec{P}-\vec{o}|} \\ \vec{U}_t &= (-U_{ry}, U_{rx}) \end{cases}$$

It follows for a distortion :

$$\begin{cases} d\vec{P}\cdot\vec{U}_r &= \frac{(P_x-x)(x-x_0)+(P_y-y)(y-y_0)}{\sqrt{(x-x_0)^2+(y-y_0)^2}} \\ d\vec{P}\cdot\vec{U}_t &= \frac{(P_y-y)(x-x_0)-(P_x-x)(y-y_0)}{\sqrt{(x-x_0)^2+(y-y_0)^2}} \end{cases}$$

and for two distortions :

$$\begin{cases} d\vec{P}\cdot\vec{U}_r &= \frac{(P'_x-P_x)(P_x-x_0)+(P'_y-P_y)(P_y-y_0)}{\sqrt{(P_x-x_0)^2+(P_y-y_0)^2}} \\ d\vec{P}\cdot\vec{U}_t &= \frac{(P'_y-P_y)(P_x-x_0)-(P'_x-P_x)(P_y-y_0)}{\sqrt{(P_x-x_0)^2+(P_y-y_0)^2}} \end{cases}$$

Contrary to K, the parameters K_r and K_t depend little on a global offset of the origins. K_r measures roughly the contribution of the magnification in a well centered K. It is positive if the second distortion is larger and negative if it is smaller. K_t measures the contribution of the rotation. It is positive for an anti-clockwise rotation and negative for a clockwise rotation. Fig. 15 shows the comparison between the optical model and the observations. K_r varies around zero level, indicating that the model does not produce a magnification systematically larger that the observations.

The parameters K_r and K_t depend little on the offset of the origin, because they are directly related to the divergence and the rotational of the vector field. K_r and $\vec{\nabla}\cdot d\vec{P}$ are related by Ostrogradski formula and K_t and $\vec{\nabla}\wedge d\vec{P}$ are related by Stockes formula. As the divergence and the rotational are derivatives, the constant offset vanishes.

$$\begin{cases} \vec{\nabla}\cdot d\vec{P} &= \frac{\partial dP_x}{\partial x} + \frac{\partial dP_y}{\partial y} \\ (\vec{\nabla}\wedge d\vec{P})_z &= \frac{\partial dP_y}{\partial x} - \frac{\partial dP_x}{\partial y} \end{cases}$$

Fig. 16 shows an example of the divergence and rotational map of a distortion polynomial pair. The sum of the divergence and rotational over the detector surface and divided by its border length (eq. 3) are quantities comparable to K_r and K_t, except that any arbitrary center in

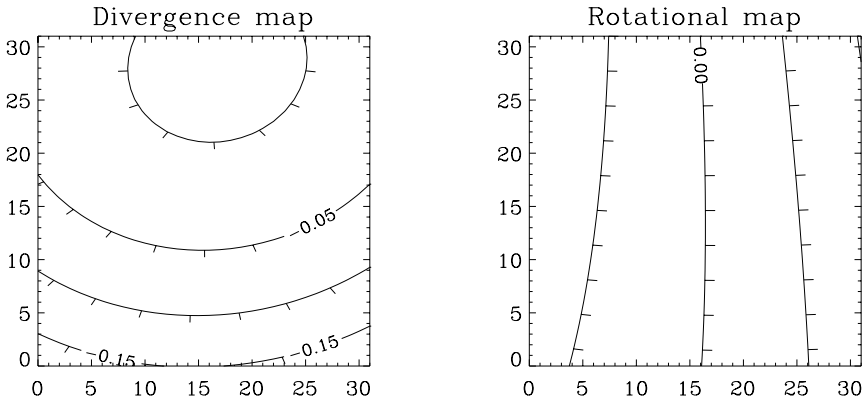

Figure 16: Divergence and rotational map of a distortion correction polynomial pair

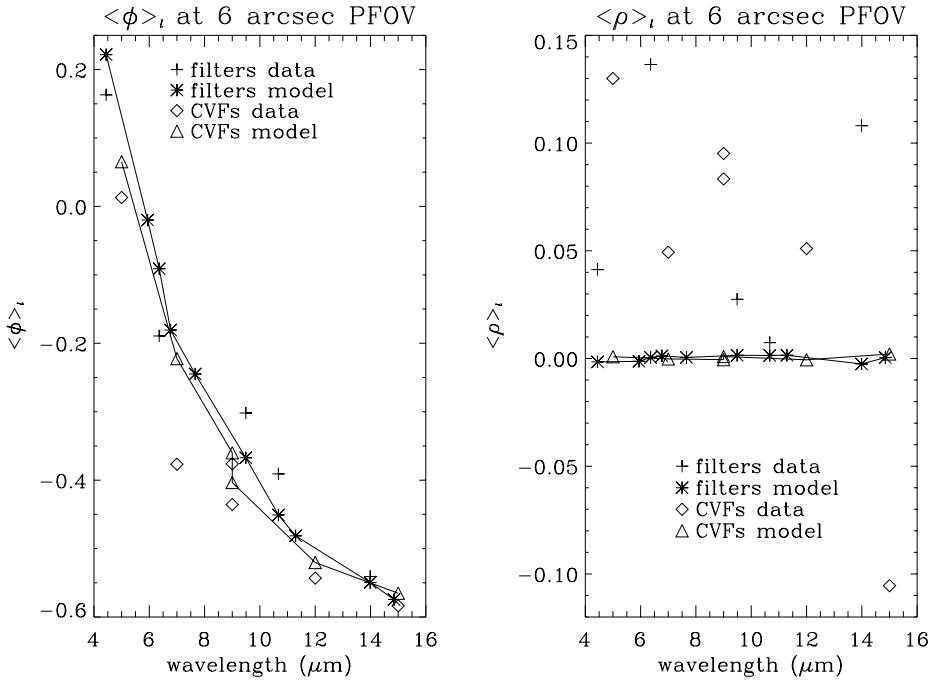

Figure 17: $< \phi >_l$ and $< \rho >_l$ of distortion correction polynomials as a function of the wavelength

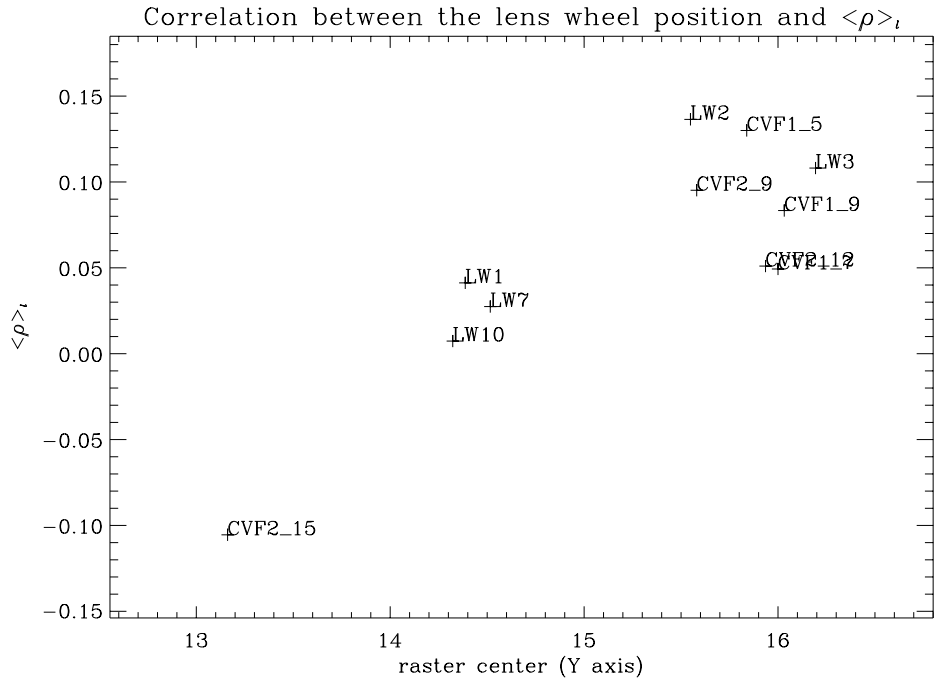

Figure 18: $< \rho >_l$ of distortion correction polynomials reflects the position of the lens wheel

necessary for the divergence and rotational.

$$\begin{cases} < \phi >_l &= \dfrac{\int_{x_{\rm inf}}^{x_{\rm sup}} \int_{y_{\rm inf}}^{y_{\rm sup}} \vec{\nabla} \cdot d\vec{P} dx dy}{2(x_{\rm sup} - x_{\rm inf} + y_{\rm sup} - y_{\rm inf})} \\ < \rho >_l &= \dfrac{\int_{x_{\rm inf}}^{x_{\rm sup}} \int_{y_{\rm inf}}^{y_{\rm sup}} (\vec{\nabla} \wedge d\vec{P})_z dx dy}{2(x_{\rm sup} - x_{\rm inf} + y_{\rm sup} - y_{\rm inf})} \end{cases} \tag{3}$$

Fig. 17 shows $< \phi >_l$ and $< \rho >_l$ of the distortion correction polynomial pairs as a function of the wavelength. The variation of $< \phi >_l$ shows what was missing in the measure of K in Fig. 14. The turn over around 6 μm seen in Fig. 14 is just an effect of the absolute value. Fig. 17 shows that the average magnification passes from positive to negative value around 6 μm. The distortion files computed from the observations listed in Tab. 1 do not include those shortward of 6 μm. Therefore, the distortion corrected image had very small amount of pixels going outside the initial detector size, whereas this becomes significant at shorter wavelengths. On the other hand, the variation of $< \rho >_l$ seems to reflect a noise rather than any significant physical parameter, at least as a function of wavelength. However, it is shown that $< \rho >_l$ shows a good correlation with a random physical parameter: the position of the lens wheel. Fig. 18 shows that the scatter of $< \rho >_l$ seen in Fig. 17 corresponds to that of the raster center which in turn is directly related to that of the lens wheel position. This scatter arises from the positioning tolerance of the lens wheel and, therefore, it is independent from the wavelength.

7 Further fine tuning of the distortion modeling

In order to perform further fine tuning of some parameters in the optical model, one has to have an idea of the error involved in the field distortion measurements.

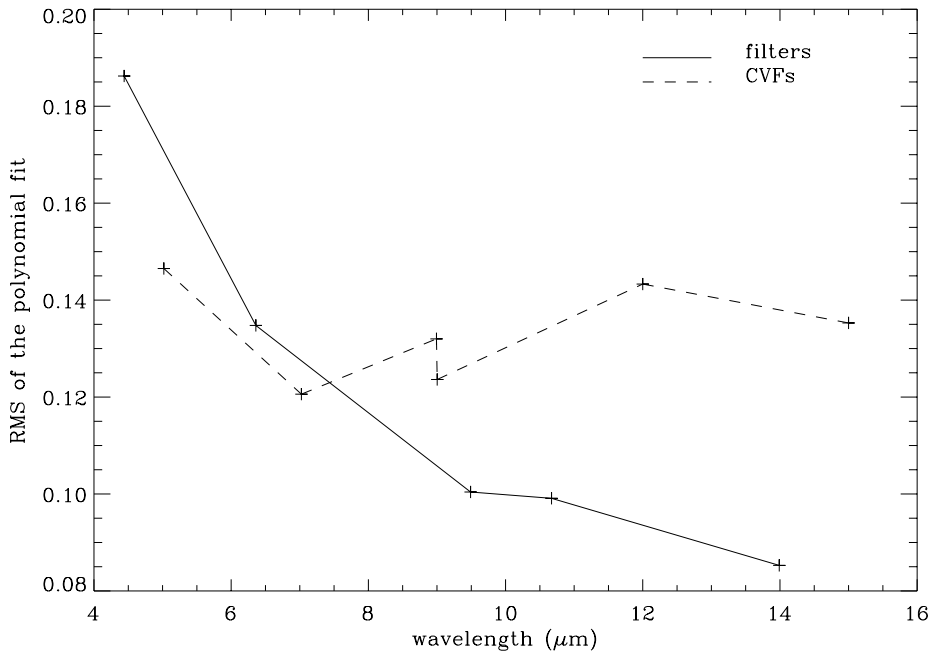

Figure 19: Standard deviation of distortion measurement relative to the fitted polynomials as a function of the wavelength

7.1 Error on the distortion measurement

Fig. 19 shows the error measured as the standard deviation of the measured raster points coordinates with respect to those given by the fitted polynomials. The measurements for filters show an increase of the error toward shorter wavelength whereas those for CVFs show no trend. The fact that the CVFs do not show a clear trend as the filters can be partly explained by their sparse raster observation. The filters have 9×9 raster points whereas the CVFs have only 9×5 (Tab. 3).

The trend shown by the filters may arise from the pixelization effect due to the poorer sampling at shorter wavelength. I define the pixelization parameter P of the measured coordinate x as:

$$P = \frac{x - \mathrm{rnd}(x_0)}{x_0 - \mathrm{rnd}(x_0)}$$

where $\mathrm{rnd}(x_0)$ means the round up value of x_0 and x_0 is the expected value of x that can be approximated by the value given by the fitted polynomials. For P smaller than the unity and near zero, the pixelization effect is severe. If P is larger than the unity or negative, the difference between x_0 and x is not due to the pixelization effect. Fig. 20 shows the fraction of the measured coordinates which satisfy $0 \leq P \leq 1$. If there is no pixelization effect, it should give a number near $1/2$. Surprisingly the filters show low fraction values at shorter wavelengths. In these ranges the values of P are mostly larger than the unity, indicating that the position measurement by PSF fit tends to draw further from a center of pixel. Even if the effect is the contrary of what is suspected, it does increase the error of measurements as well. Therefore, the larger standard deviation seen in Fig. 20 at short wavelength is due to the error on the measurements rather than the intrinsic limit of the third order polynomials to fit the distortion pattern. Fig. 19 gives an idea of the minimum error one can reach in the distortion measurements.

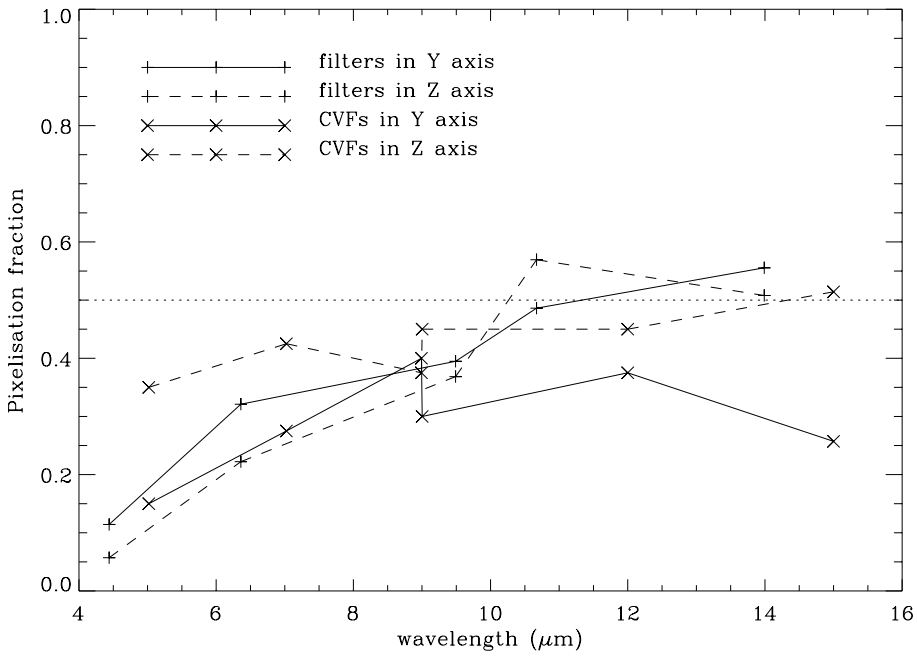

Figure 20: Fraction of the measured positions which are attracted towards the pixel center

7.2 Influence of the lens wheel position on the field distortion

As suspected earlier (Fig. 1), different positions of the lens wheel in the limit of tolerance give different distortion patterns. This effect can be simulated by the optical model. The most obvious example is shown with 12 arcsec PFOV lens (Fig. 21). The difference is much smaller with 6 arcsec PFOV lens, but it does show a slight difference between the two extreme positions (Fig. 22).

Theoretically the extremum of the divergence should be directly related to the position of the lens wheel. However, this extremum is located in the area of minimum distortion which may be smaller than the accuracy of the point source position measurement. This implies that the position of the extremum is very sensitive to the noise in the measurement. Fig. 23 shows a very large scatter compared with the parameter $< \phi >_l$ in Fig. 18 which, on the contrary, is measured in the area of the detector where the distortion is strongest.

Fig. 24 shows an example of the distribution of the difference $\Delta(x, y)$ of the distortion correction between the observations and the model.

$$\Delta(x,y) = \sqrt{(P'_x(x,y) - P_x(x,y))^2 + (P'_y(x,y) - P_y(x,y))^2}$$

In general, the difference is minimum in the central area, and it reaches the maximum somewhere on the edges. The maximum difference $\Delta_{\max}$ inside the detector surface is an important quantity for the distortion modeling, since it may indicate the maximum error when using the distortion correction derived from the optical model. The difference of the lens wheel position between the observed data and the model is computed based on the parameter $< \phi >_l$ and the correction is applied. In general, $\Delta_{\max}$ decreases after the lens wheel position crrection. Fig. 25 shows $\Delta_{\max}$ after the correction as a function of wavelength. The typical value is quite large : ≈ 0.3 of the pixel size.

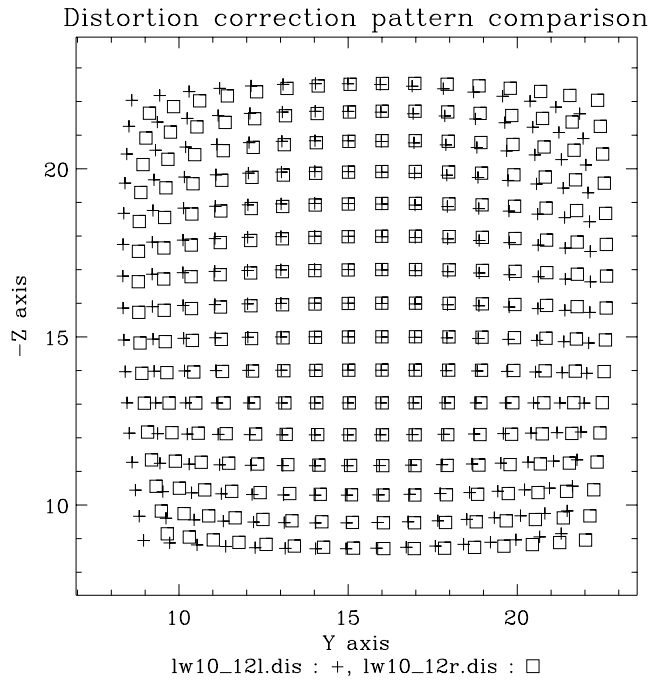

Figure 21: Simulated distortion correction pattern for two extreme positions, left and right, of the 12 arcsec PFOV lens

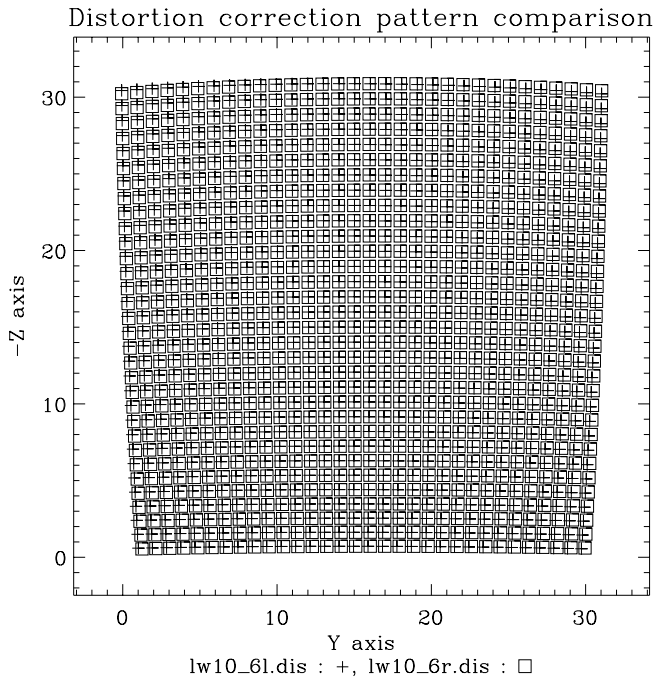

Figure 22: Simulated distortion correction pattern for two extreme positions left and right, of the 6 arcsec PFOV lens

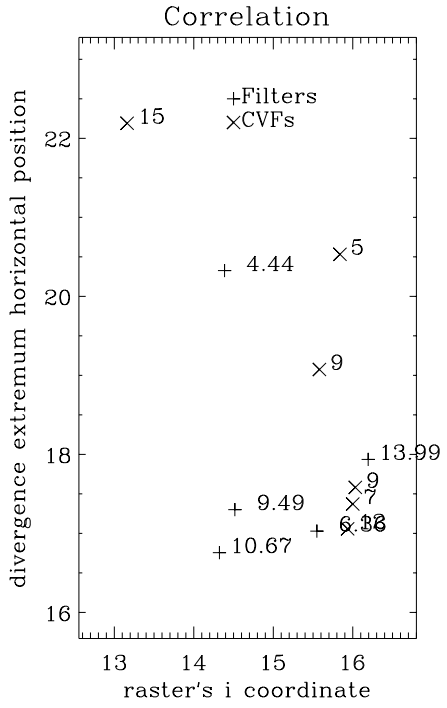

Figure 23: Correlation between the horizontal coordinates of the center of the raster the divergence extremum

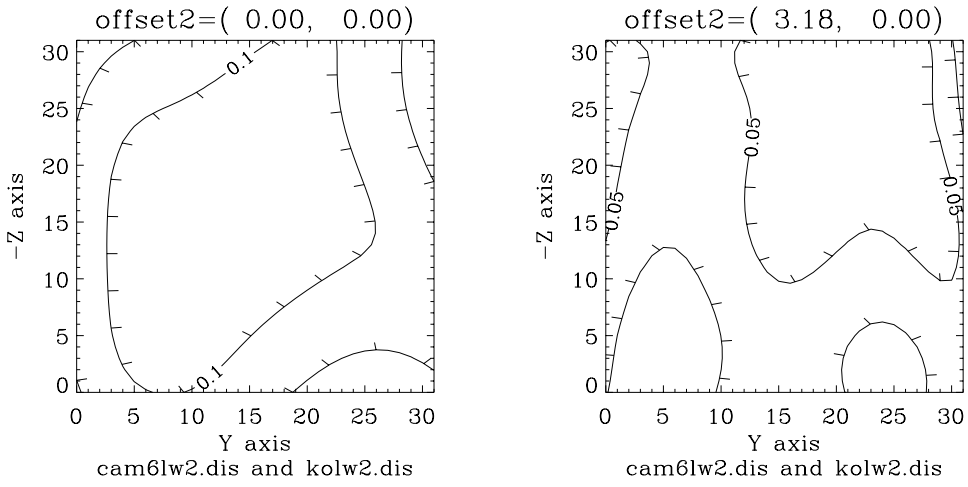

Figure 24: Examples of difference map between the data based and the model based distortion correction polynomials. An offset of the distortion pattern improves the distortion model.

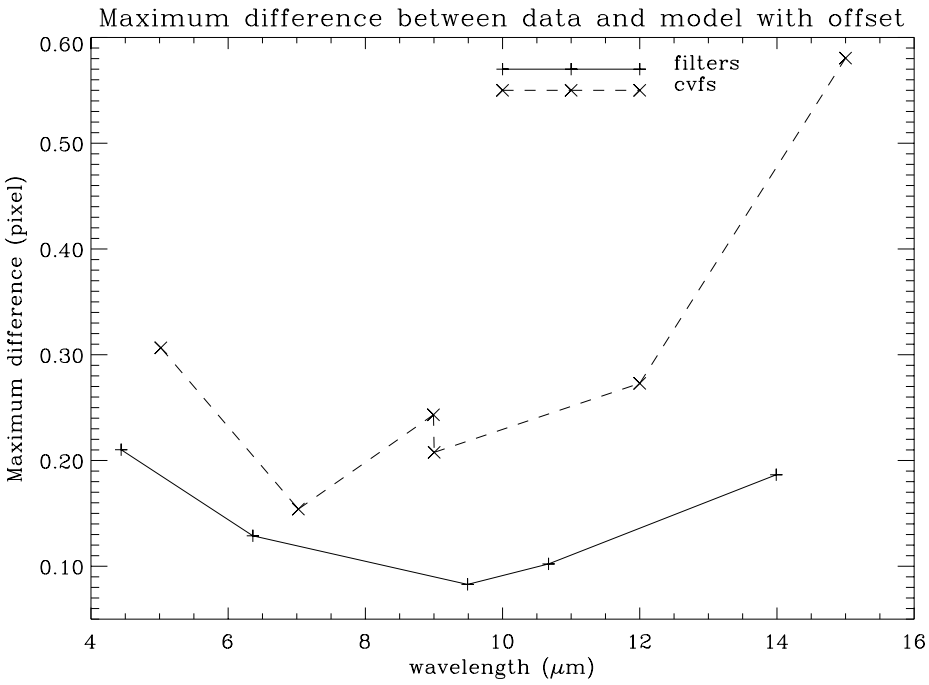

Figure 25: After applying to the model an offset determined by $< \phi >_l$ criteria, the maximum difference between the data and the model is reduced to a third of a pixel, except for a CVF at 15 μm

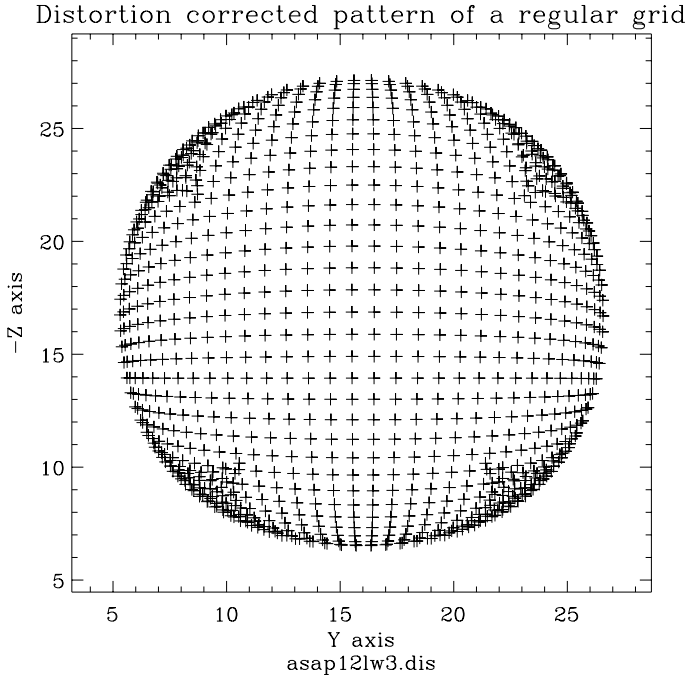

Figure 26: An example of the polynomial behaviour outside the field of view (optical simulation with 12 arcsec pfov lens)

Table 5: Retained number of positions and their mean signal to noise ratio in the distortion measurements

6" data	positions	mean S/N	simulated Δ_{max}	measured Δ_{max}
LW1 ghost	70	421	0.40	0.21
LW2 ghost	81	787	0.35	0.17
LW7 ghost	76	393	0.25	0.13
LW10 ghost	72	397	0.40	0.12
LW3 ghost	63	468	0.30	0.18
CVF1 at 5 μm ghost	40	312	0.70	0.29
CVF1 at 7 μm ghost	40	212	1.00	0.34
CVF1 at 9 μm ghost	40	231	0.40	0.26
CVF2 at 9 μm ghost	40	287	0.40	0.22
CVF2 at 12 μm ghost	40	170	0.35	0.25
CVF2 at 15 μm ghost	35	232	0.45	0.64
New LW1 data	266	4	0.65	0.60
New LW2 data	4768	14	0.10	0.24
New LW10 data	67	11	1.40	0.99
New LW3 data	1294	26	0.15	0.15

In general, the parameter Δ_{max} corresponds to the difference of the outermost limit of the detector area. If a set of measured star positions does not extend far enough until the detector edges, the polynomial fit may deviate quickly between the outermost data points and the detector edges. In Fig. 10, it is obvious that a third order polynomial has a turn around point outside both sides of the image border, which deviates rapidly from a realistic distortion pattern. Fig. 26 is an example of 12 arcsec pfov lens showing what happens to the distortion correction polynomials outside the area of fit.

The only way of decreasing Δ_{max} level might be to decrease this error by a statistical way, using other sets of observations with more point sources observed over the field of view.

7.3 Extended data set

New sets of observations have been selected and reduced to try to reach a better estimate of the field distortion (Ott et al. 2001 [5]). These data sets provide a larger number of star positions, but their signal to noise ratios are often very small compared to those of the ghost measurement data. Tab. 5 lists all the data used with their estimated quality. The number of star positions used in the new LW2 data is larger by a factor of hundred than the ghosts measurement data, whereas their mean signal to noise ratio is smaller by a factor of ten.

The LW2 and LW3 data provide enough star positions uniformly spread all over the detector surface, giving us the first opportunity to estimate the goodness of the point source position determination by the PSF fitting. The results is quite meaningful. The left contour map of Fig. 27 shows the distribution of the fractional part of the positions determined by the PSF fitting routine on the LW2 data using the computed LW2 PSFs. The routine tends to give systematically a position towards a corner of the pixel. This bias is due to the fact that the computed PSFs are narrower than the observed ones at short wavelength. The right contour map of Fig. 27 also shows the distribution of the error inside a pixel, when fitted with the

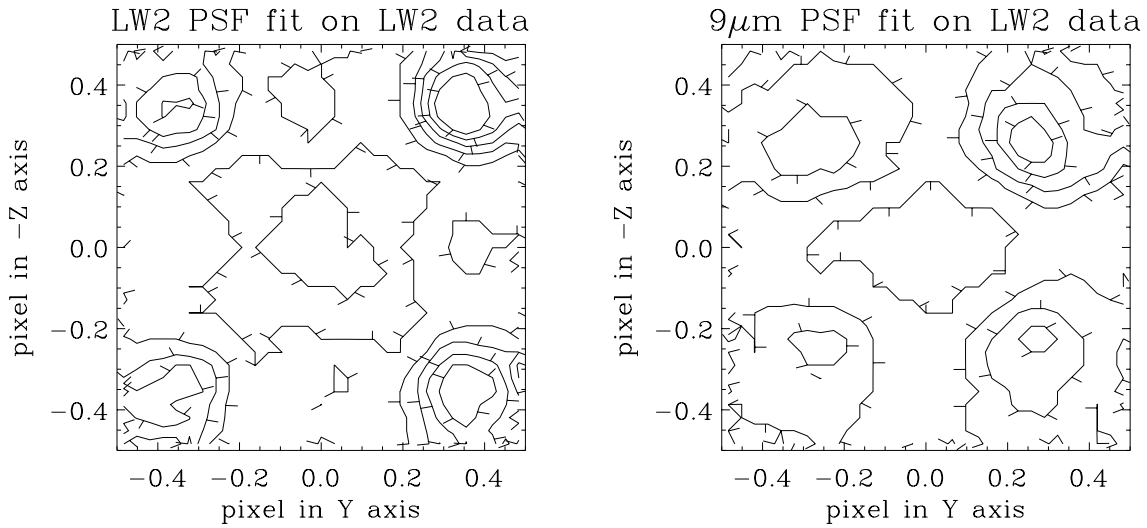

Figure 27: Non Gaussian systematic error due to the PSF fitting bias with LW2 filter. The contours are 5, 92, 183, 275, 366 and 457×10^{-4}% for both maps.

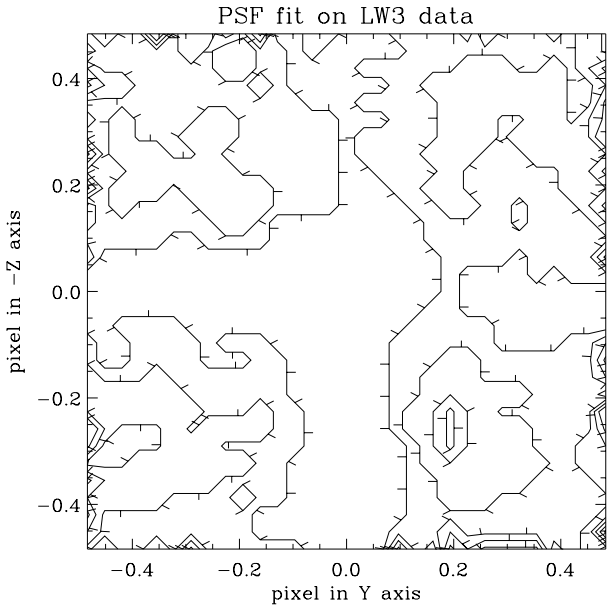

Figure 28: Non Gaussian systematic error due to the PSF fitting bias with LW3 filter. The contours are 5, 13, 22 and 30×10^{-2}% for both maps.

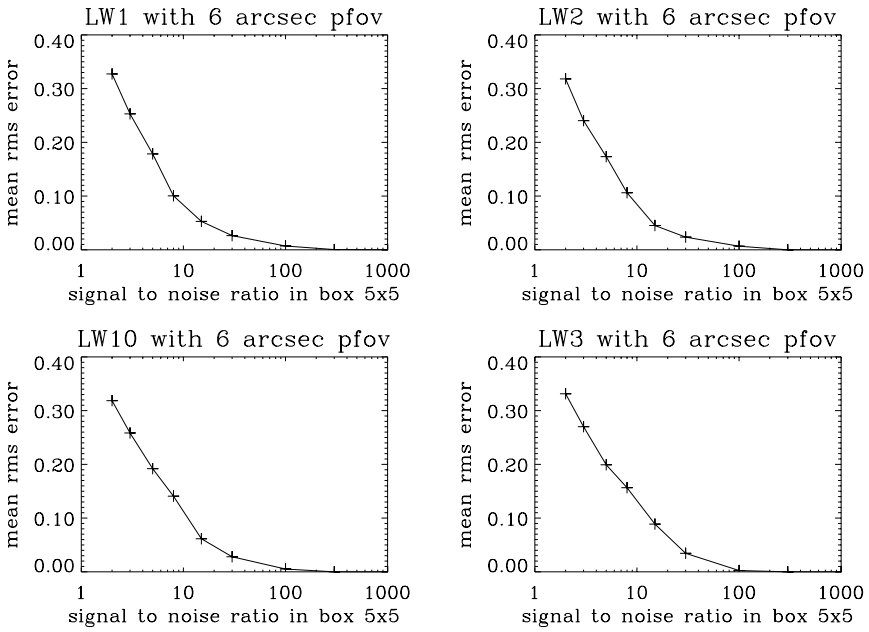

Figure 29: Simulations of the point source position error as a function of the signal to noise ratio, when the PSF fitting is used.

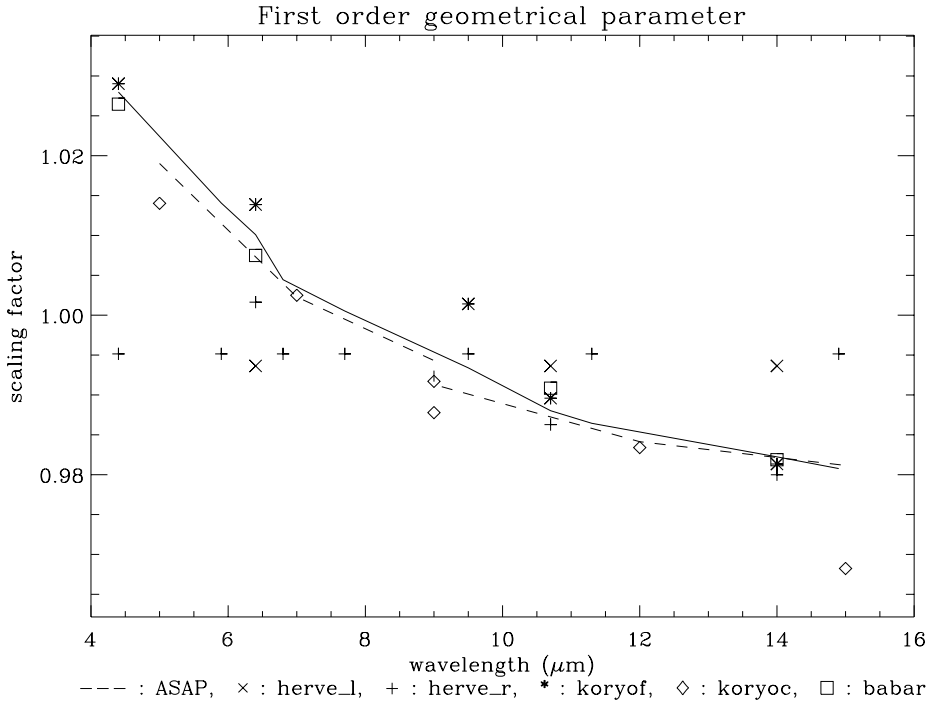

Figure 30: Scaling factor of the distortion correction polynomials with respect to the detector center. + : Aussel's right files, x : Aussel's left files, * : filters of previous section, ◇ : CVFs of previous section, □ : new data sets, solid line : filters model, dashed line : CVFs model.

computed 9μm PSFs. The effect still remains, but the maxima are located a little more towards the center of the pixel, and the peaks are lower than the previous case. Fig. 28 shows the case with LW3 filter. The PSF fitting bias is still seen at this 15μm wavelength, but at lower levels with smaller gradient. Although with a poorer statistics, this bias effect is also clearly seen in the ghosts measurement data. The result shown in Fig. 20 which is presented as the negative pixelization effect arises from this same bias.

The fourth column in Tab. 5 shows $\Delta_{\max}$ derived from the statistics of simulations. The parameter $\Delta_{\max}$ depends strongly on the distribution of the star positions on the detector and their signal to noise ratios. Thus, it should be estimated case by case. In order to estimate it, some simulations have been performed by taking into account the distribution of the star positions, the signal to noise ratio of each source (also estimated by simulations Fig. 29) and also the systematic error of the PSF fit bias which arises from the discrepancy of the theoretical and observed PSFs.

Fig. 30 shows the comparison of all the derived polynomials in terms of the magnification parameter computed from the linear terms of the polynomials. It is clearly seen that the most of the Aussel's files are aligned around a value of 0.995, because the wavelength dependency was ignored at that time and the files had been directly copied from the available data set of that time. The the model follows reasonably result of the other measurements. The largest deviation is seen for the CVF at 15 μm probably due to its small number of retained positions as seen in Tab. 5.

References

[1] H. Aussel ISOCAM LW Channel Field of View Distortion 1998, Technical report

[2] H. Aussel ISOCAM Field of View Distortion Measurements and Correction 1999, ISOCAM Calibration Workshop

[3] K. Okumura ISOCAM PSF Report 1998, Technical report

[4] K. Okumura, M. Pérault, Y. Longval and F. Sibille Ghosts in ISOCAM images 1998, Technical report

[5] S. Ott, A. Babar, R. Gastaud and K. Okumura, ISOCAM field distortion. in preparation, 2001